*Chapter in* **Advancing Astrophysics with the SKA – II**

# Deep H I observations of cold gas inflow and outflow

W.J.G. de Blok,[1,2,3] D.B. Fisher,[4,5] K. Tachihara,[6] F.M. Maccagni,[7,8] J. Wang,[9] R. Enokiya,[10] L. Chemin,[11] T. Hayakawa,[6] D. Kleiner,[1] D.J. Pisano[2] and S.H. Oh[12]

[1]*Netherlands Institute for Radio Astronomy (ASTRON), Oude Hoogeveensedijk 4, 7991 PD Dwingeloo, the Netherlands*

[2]*Dept. of Astronomy, Univ. of Cape Town, Private Bag X3, Rondebosch 7701, South Africa*

[3]*Kapteyn Astronomical Institute, University of Groningen, PO Box 800, 9700 AV Groningen, The Netherlands*

[4]*Centre for Astrophysics and Supercomputing, Swinburne University of Technology, Hawthorn, VIC 3122, Australia*

[5]*ARC Centre of Excellence for All Sky Astrophysics in 3 Dimensions (ASTRO3D)*

[6]*Department of Physics, Graduate School of Science, Nagoya University, Furo-cho, Chikusa-ku, Nagoya, 464-8602, Japan*

[7]*INAF – Osservatorio Astronomico di Cagliari, via della Scienza 5, 09047, Selargius (CA), Italy*

[8]*Wits Centre for Astrophysics, School of Physics, University of the Witwatersrand, 1 Jan Smuts Avenue, 2000, Johannesburg, South Africa*

[9]*Kavli Institute for Astronomy and Astrophysics, Peking University, Beijing 100871, China*

[10]*National Astronomical Observatory, Japan, 2-21,-1, Osawa, Mitaka, Tokyo, 181-8588, Japan*

[11]*Université de Strasbourg, CNRS, Observatoire Astronomique de Strasbourg, UMR 7550, 67000 Strasbourg, France*

[12]*Department of Physics and Astronomy, Sejong University, 209 Neungdong-ro, Gwangjin-gu, Seoul, Republic of Korea*

A major question in galaxy evolution is how galaxies acquire sufficient gas to sustain their star formation rates. H I observations with high angular resolution and sensitivity to very low column densities are some of the important observational ingredients that are currently still missing. Answers to these questions are necessary for a correct interpretation of observations of galaxy evolution in the high-redshift universe and will provide crucial input for the sub-grid physics in hydrodynamical simulations of galaxy evolutions. In this chapter we discuss the progress that has been made over the past years, describe the various processes that lead to inflow and outflow of gas, and discuss how SKA-Mid AA4 observations can contribute to further understanding these important aspects of galaxy evolution using deep observations of nearby individual disk and dwarf galaxies.

 

## 1 Ultra-deep H I observations with SKA-Mid

Galaxy evolution is driven by the flow of gas into galaxies, the transformation of gas into stars, and the expulsion of gas due to the subsequent stellar evolution processes. Atomic neutral hydrogen (H I) is an excellent tracer — and often the main constituent — of this gas component, and can be observed in the 21-cm line. The SKA will be able to trace the gradual transformation from primordial hydrogen into galaxies over cosmic time. It will provide direct and detailed observations of the physical processes that cause this transformation and which will help to correctly interpret this evolution.

An important process in this is gas accretion. It delivers gas from outside galaxies (either primordial or previously ejected) into the star-forming disks, which ensures galaxies can keep forming stars over a Hubble time. In general, local galaxies only have enough gas to sustain their SFR for few Gyr, and they must thus acquire gas from somewhere else (see Sancisi et al. 2008 for an overview). One of the ways in which gas can flow onto the star forming disk is through "cold accretion" where numerical simulations have predicted that gas flows in from the intergalactic medium (IGM) (or "cosmic web") (e.g., Kereš et al. 2005). "Cold" in this context means that the gas has not been shock-heated as it entered the galaxy halo. So far there is little direct observational evidence for significant cold accretion. The observed cold gas accretion in galaxies seems to be an order of magnitude too low to explain the current star formation rates (SFR) in galaxies (Sancisi et al., 2008; Putman et al., 2012). An alternative accretion path is through the galactic fountains. These propel gas into the halo, which rains back on the disk, dragging additional gas back in (Fraternali, 2017).

If cold accretion as predicted by the simulations is the dominant process by which galaxies acquire their gas, then current observational limits indicate it must happen at H I column densities below $\sim 10^{18}$ cm$^{-2}$ (Marasco et al., 2025), based on recent deep MeerKAT observations obtained as part of the MHONGOOSE (MeerKAT H I Observations of Nearby Galactic Objects: Observing Southern Emitters) survey (de Blok et al., 2024). At these low column densities, the H I is of course no longer the main mass component of the accretion flow, but serves as a tracer.

As part of the galactic fountain process (Shapiro and Field, 1976; Bregman, 1980; Norman and Ikeuchi, 1989), massive stars, through supernova explosions and stellar winds, can push gas out of the disk and into the halo of a galaxy. This creates the holes and bubbles frequently observed in the gas disks of galaxies (Bagetakos et al., 2011). The expelled gas will cool and eventually rain back on the disk, most likely in the form of H I clouds (Putman et al., 2012). Such clouds have also been observed in a number of other galaxies as part of an extra-planar gas component (Sancisi et al., 2008), and presumably form the equivalent of the high and intermediate velocity clouds (HVCs and IVCs, respectively) in our Galaxy. It is thought that the process of these clouds moving through the hot gaseous halo of a galaxy provides an alternative mechanism for accretion of gas. Here, hot halo gas cools in a cloud's wake and is dragged along as the cloud moves back into the disk (Fraternali, 2013).

The current state of the art in attempting to detect low-column density H I around nearby galaxies is the MHONGOOSE survey. This is a MeerKAT survey of 30 nearby disk and dwarf galaxies, detecting H I column densities down to $\sim 5 \times 10^{17}$ cm$^{-2}$ using 55 hours of integration time per

galaxies. To date this is the deepest targeted H I survey of nearby galaxies. Some of the early results of this survey include the discovery of a large number of low-mass dwarf galaxies around our target galaxies. With H I masses of a few times $10^6$ $M_\odot$, these are the equivalents of Local Group dwarfs, which can now be detected out to $\sim$ 20 Mpc with MHONGOOSE (Maccagni et al. 2024). Another early discovery is the presence of a low-column density outer disk component around NGC 5068. There is no clear origin for this gas, so this may indicate accretion from the IGM, as also hinted at by the metallicities of star forming regions (Healy et al 2024). Stacking of the MHONGOOSE data show no strong evidence for the presence of extensive low-column density material (Veronese et al 2025). This supports the analysis by Marasco et al. (2025) who conclude that the infalling cool gas filaments predicted as part of the cold accretion process should have been detected by MHONGOOSE. This incomplete list shows the impact of the dramatic increase in quality of the MeerKAT data over previous studies.

As an illustration of the quality we show in Fig. 1 an overview of the H I distribution of four MHONGOOSE galaxies each differing by about an order of magnitude in H I mass. The progression from low to high star formation rates, and the increasing orderedness of the disks is clearly visible. As will be discussed below, these data already give us a very clear idea of what a typical SKA-Mid observation of a nearby galaxy will look like.

### 1.1 SKA Prospects

In order to plan and eventually execute SKA observations it is important to have a good overview of the column densities and resolutions that can be reached with SKA in a reasonable time. A first indication of this was already given in de Blok et al. (2024) and additionally in Maccagni and de Blok (2024). There, a comparison was made between (homogenized) column density sensitivities and resolutions of past targeted H I surveys and those expected to be reached by SKA. In those papers, a preliminary SKA design was used. Here we revisit this comparison, but this time using the actual predictions of the SKA-Mid sensitivity calculator made available by SKAO. This comparison is shown in Fig. 2. Interferometric targeted surveys shown here are The H I Nearby Galaxy Survey (THINGS; Walter et al. 2008), the Hydrogen Accretion in LOcal GAlaxieS survey (HALOGAS Heald et al. 2011), the Westerbork H I Survey Project (WHISP; van der Hulst et al. 2001), the Local Irregulars That Trace Luminosity Extremes, The H I Nearby Galaxy Survey (LITTLE THINGS; Hunter et al. 2012) and the Local Volume H I Survey (LVHIS; Koribalski et al. 2018). Also shown is the untargeted Widefield ASKAP L-band Legacy All-sky Blind surveY (WALLABY; Koribalski et al. 2020). For the single-dish observations we show the column density sensitivities for the H I Parkes All Sky Survey (HIPASS; Barnes et al. 2001; Meyer et al. 2004), the Arecibo Legacy Fast ALFA (ALFALFA; Haynes et al. 2018), the Arecibo Galaxy Environment Survey (AGES; Auld et al. 2006), deep observations of M31 (Wolfe et al., 2016) and NGC 2903 (Irwin et al., 2009), as well as a number of deep GBT and Parkes observations of nearby galaxies (Sorgho et al. 2019, Sardone et al. 2021, Pingel et al. 2018). We also show deep H I observations taken with the Five-hundred-meter Aperture Spherical Telescope (FAST) as part of the FAST Extended Atlas of Selected Targets Survey (FEASTS; Wang et al. 2024).

To ensure a proper comparison we have taken the noise per channel and the channel widths from the source papers or the corresponding publicly available data and homogenized these quantities

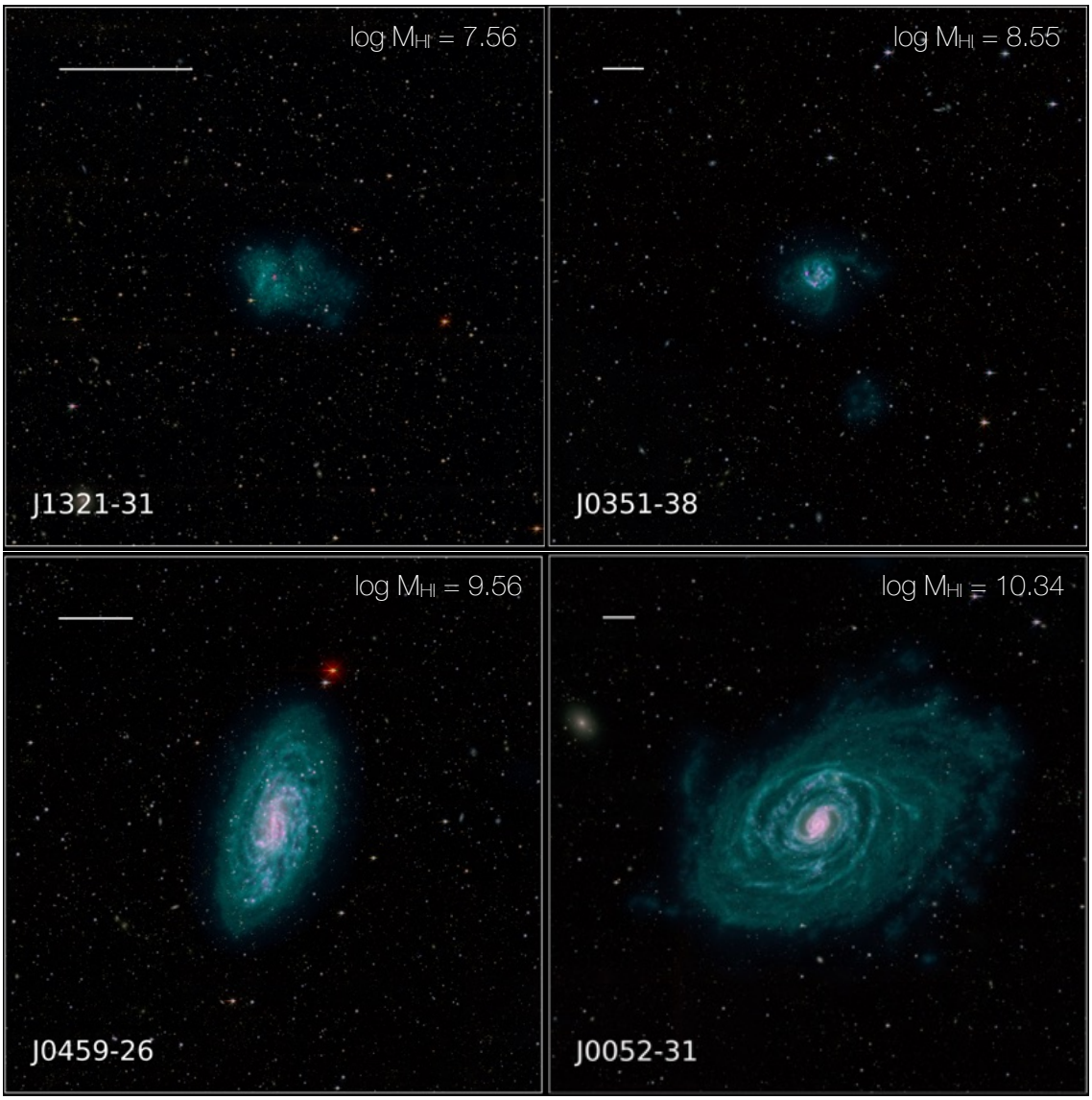


**Figure 1:** MHONGOOSE H I distributions (cyan), combined with Galex UV (pink) and Legacy Survey optical images (background) of four sample galaxies each differing about an order of magnitude in H I mass. A 10 kpc scale bar is shown in the top-left of each panel, the H I mass in the top-right. The HIPASS identification is shown in the bottom-left. These correspond to (top-left to bottom-right) KK98-195, ESO 302-G014, NGC 1744 and NGC 289.

to a common channel width of 16 km $s^{-1}$, assuming square-root scaling of noise with channel-width. A 16 km $s^{-1}$ channel width corresponds approximately to the FWHM of an H I line with a velocity dispersion of 7 km $s^{-1}$, which is comparable to the lowest values seen in previous H I observations of nearby galaxies (Ianjamasimanana et al., 2017). Also shown are the sensitivities reached by MHONGOOSE, the deepest targeted H I survey of nearby galaxies to date with 55 hours of MeerKAT observing time per galaxy. We also show the sensitivities that will be reached by the SKA-Mid AA* and AA4 arrays for observing times of 10 hours and 100 hours. The noise levels and beam sizes were derived using the early 2025 version of the official SKAO SKA-Mid sensitivity

calculator[1] where we assumed a source at zero redshift (frequency 1420 MHz), a spectral resolution of 1.4 km s$^{-1}$, with the source at a declination of $-30°$. For reasons of clarity, we only show the column density sensitivities that will be achieved using robust weighting with robustness parameter of 1.0. The different resolutions shown in the Figure are achieved by tapering. Values derived using different weightings generally lie within 0.2 dex of the curves shown. We note one difference between the SKA resolutions shown in this Figure and the ones derived by the sensitivity calculator. We found that for higher robust values ($\gtrsim 0.5$) and small beam sizes ($\lesssim 6''$) the output beam sizes as derived by the calculator underestimated the size of the PSF. We re-derived the PSF based on the *uv* distribution of the observations shown, and found PSF sizes that were typically larger by up to a factor of 2.

There are three aspects of Fig. 2 that are worth noting. The first is the almost complete overlap of the MHONGOOSE curve and the SKA 10h curves. Essentially, this shows that a 50 hour observation with MeerKAT is as sensitive as a 10 hour observation with SKA-Mid. In other words, the current MHONGOOSE observations already give us a preview of what can be expected from SKA-Mid in 10 hours in terms of H I emission observations of the nearby universe. The second aspect is the location of the AA* and AA4 curves with respect to each other. AA4 contains more dishes than AA*, but as these are preferentially located at large distances from the core (i.e., longer baselines), their contribution to the column density sensitivity is limited. It should be stressed, of course, that this is strictly only the case for H I emission. For H I absorption and continuum observations there will be a big difference in resolutions that can be achieved. The third aspect is that in order to observe a truly unexplored part of resolution-column density parameter space, observing times of $\sim$ 100 hours or more are essential.

With a survey speed that is five times better than MeerKAT, SKA-Mid will enable detailed and resolved statistical studies of the low-column density H I in the local universe. With the same amount of observing time as it took to do MHONGOOSE, SKA-Mid can map in the same detail a sample of 150 galaxies, rather than the 30 that were done with MeerKAT. At the higher resolutions, SKA-Mid is somewhat more sensitive than MeerKAT, meaning that MHONGOOSE depth can be achieved at $\sim 5''$, rather than the $8''$ of MHONGOOSE. A 100h integration improves the column density sensitivity by 0.5 dex, bringing us in an unexplored regime. It also enables observations to MHONGOOSE depth, but at a resolution that is a factor $\sim$ 2 higher. Resolving the low-column density gas spatially may be key to further constraining the processes that govern gas accretion. In the following we discuss some of these processes in more detail.

## 2 Cold gas outflows and the regulation of mass growth in galaxies

### 2.1 The true mass-loss from outflows requires H I observations of starburst galaxies

Feedback, from both star formation and active galactic nuclei, is among the most important mechanisms driving galaxy evolution. Energy and momentum from strong radiation fields, AGNs and supernovae push gas out of the disk plane, reshaping the galaxy and its surroundings. In galaxies like the Milky Way and nearby spirals, this process forms arc-like superbubbles (e.g. Mac Low

[1] `https://sensitivity-calculator.skao.int/`

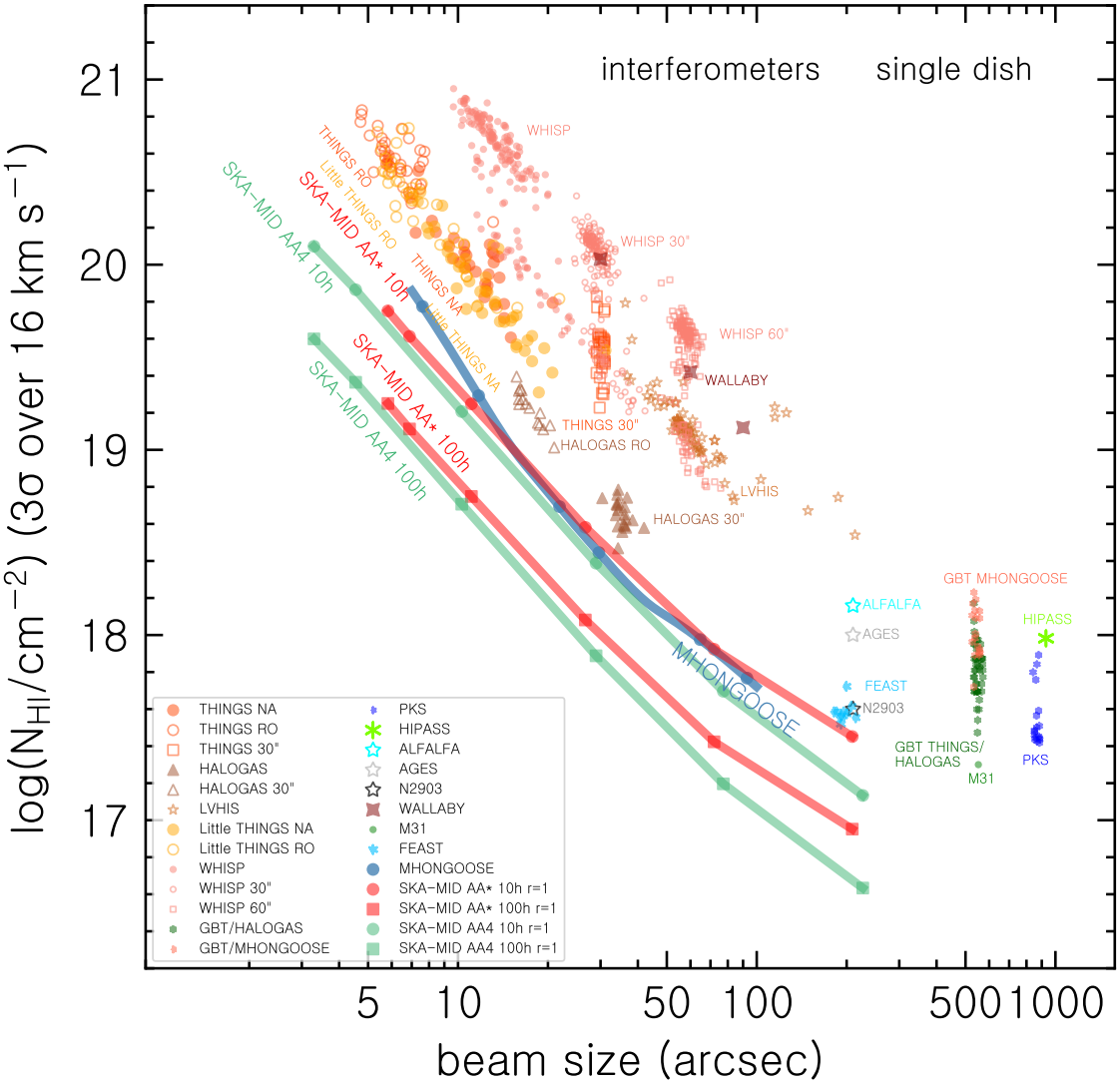


**Figure 2:** Sensitivity versus resolution in H I surveys. Colored symbols show the $3\sigma$ column density sensitivity over 16 km s$^{-1}$ for various interferometric and single-dish surveys, as indicated by the labels and legend and listed in the text. The thick blue line shows the observed MHONGOOSE sensitivities. MHONGOOSE reaches single-dish sensitivities but at a 10–50 times better angular resolution. To give an indication of the physical scales: at 10.3 Mpc (the median distance of the MHONGOOSE sample), 10″ corresponds to 0.5 kpc. Galaxies that are part of a sample with a fixed angular resolution (THINGS 30″, GBT, PKS, FEASTS) were given small, random horizontal offsets for clarity. References are given in the text.

et al., 1989), while in more intense starbursts or strong AGNs it generates galaxy-scale superwinds (Veilleux et al., 2005) that transport gas deep into the circumgalactic medium (CGM). Through this gas removal, feedback regulates the mass growth of galaxies. Simulations tell us that without this ejection of gas from galaxies there would be of order 10-100× greater stellar mass (Pillepich et al., 2018). These winds are therefore critical to setting the properties of the CGM (Tumlinson et al., 2017). While in the local Universe very few galaxies drive superwinds, all evidence suggest that

winds were essentially ubiquitous in star forming galaxies at $z \sim 1-4$ (reviewed by Förster Schreiber and Wuyts, 2020). The current-day mass and overall properties of local Universe galaxies, like the Milky Way, are dependent on the physical mechanisms in those outflows which they experienced in the past.

Many fundamental questions remain on exactly how this process works (Thompson and Heckman, 2024), with a large amount of uncertainty surrounding the cold gas phases (neutral atomic and molecular) of the wind (Veilleux et al., 2020). Cold gas, the fuel for star formation, plays a critical role in this regulation. If larger amounts of cold gas launch from a galaxy, then star formation more effectively self-regulates. The relative mass-loss rate from outflows per star formation rate in the galaxy provides a key test to large cosmological simulations (Nelson et al., 2019; Pandya et al., 2021) as well as high-resolution simulations (e.g. Kim et al., 2017; Rathjen et al., 2021). These simulations make a clear prediction that more massive galaxies, with more star formation, remove gas less efficiently (lower $\dot{M}_{out}/SFR$). Moreover, Wright et al. (2024) show that the properties of the winds more strongly constrain subgrid physics in simulations, than do bulk properties like the mass functions of the galaxy. Measurements of the true galactic wind mass-loss rates, therefore, shape our understanding of galaxies.

More than a decade after ALMA enabled some of the first resolved views of CO in winds (Bolatto et al., 2013), the amount of cold gas in winds remains very uncertain. Because most work has focused on individual, nearby targets very little information is available on the general relationships between outflow mass loss and driving properties such as the star formation rate, mass and general properties of the galaxy. This is needed to constrain theory. To date there are only a handful of galaxies with well-resolved observations of H I in outflows (e.g. Oosterloo et al., 2007a; Johnson et al., 2012; Martini et al., 2018; Mazzilli Ciraulo et al., 2025). This challenge has been due to the combined need for sensitivity and spatial resolution from radio interferometers. SKA, therefore, stands to make a leap forward in progress of this subject.

Figure 3 shows the H I gas in and around two of the nearest starburst galaxies, M82 and NGC 1569. In both galaxies, recent and ongoing star formation generates sufficient energy to force gas out of the galaxy into the surrounding circumgalactic medium. The images show how H I gas extends in 4-8 kpc long streams of material from the minor-axis. The H I substructure takes a U-shape on both sides of the galaxy, consistent with the multiphase model of outflows in which a hot X-ray cone of gas fills in the central part and heats any colder material (e.g. Leroy et al., 2015). Modelling of the M 82 outflow suggests that the cold gas dominates the wind (Xu et al., 2023; Yuan et al., 2023), with H I as possibly the largest mass component. This is likewise true in recent analysis of NGC 1569 (Mazzilli Ciraulo et al., 2025). These starbursts are extremely different, M82 is more massive by a factor of 10 than NGC 1569 and is a highly metal-enriched system, while NGC 1569 is a low mass galaxy with metallicity of $Z \sim 0.2\ Z_{\odot}$. Given that so few galaxies have H I , X-ray and ionised gas outflow measurements, the current data suggests that H I dominated winds are common, but this requires testing.

Fig. 4 compares the so-called “mass-loading" of outlows ($\eta = \dot{M}_{out}/SFR$) to the stellar mass of galaxies for the three galaxies that have measured H I and ionised gas mass outflow rates. The relationship between the mass-loading and galaxy properties provides one of the strongest tests to

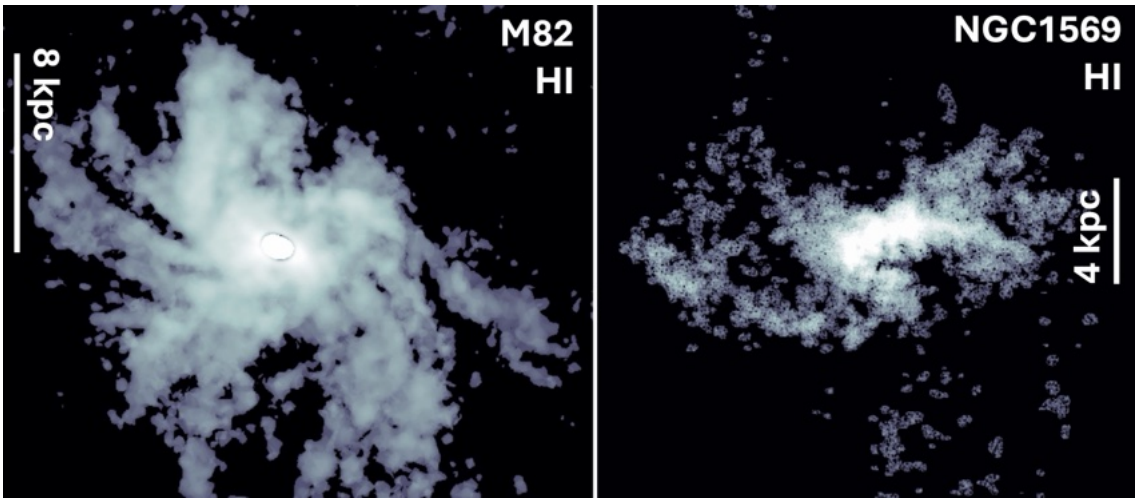


**Figure 3:** H I moment 0 maps from VLA observations of the nearest, accessible outflow systems, M 82 (left, Martini et al., 2018) and NGC 1569 (right, Johnson et al., 2012). In both cases streams of H I extend away from the disk of the galaxy. These galaxies are understood from optical and X-ray observations to be driving large scale winds (review in Veilleux et al., 2005, 2020), and the H I observed perpendicular to the disk is likely significant mass-loss from each galaxy. The nearby proximity of these targets (~3.2 Mpc for both) is key to mapping H I with current radio facilities.

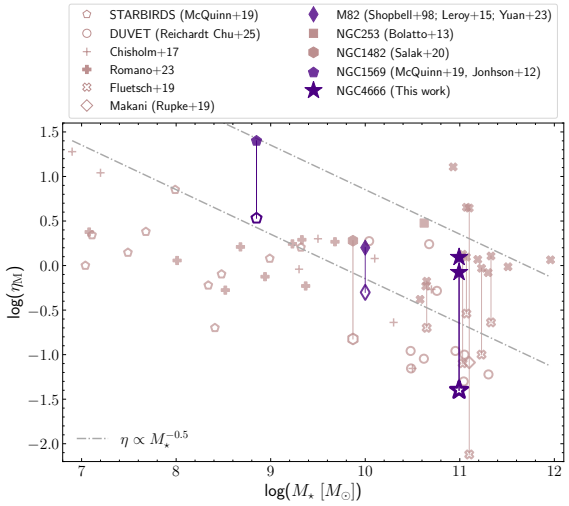


**Figure 4:** Mazzilli Ciraulo et al. (2025) compares ionised gas to H I mass outflow rates in all 3 galaxies that have resolved observations of each. All current data suggests that H I dominates that mass-outflow rate by a factor of $\sim 5-10\times$ over the warm ionised gas. The trend in the relationship of $\dot{M}_{out}/SFR$ with $M_{star}$ is a direct test of galaxy evolution models (Pandya et al., 2021; Wright et al., 2024).

galaxy evolution models (Wright et al., 2024). It is therefore critical to determine the full mass leaving the disk. While there are hundreds of measurements of unresolved ionised gas mass-loading in galaxies (Förster Schreiber and Wuyts, 2020), and likewise recent integral field spectroscopic programs are now creating resolved observations of tens of outflows (e.g. Reichardt Chu et al., 2025), there are to date very few resolved measurements of H I outflows. Fig. 4 illustrates that

H I strongly dominates the mass leaving a galaxy. H I represents the fuel for future star formation; this is different for ionised gas. H I is, therefore, a more direct tracer of the impact of outflows on the regulation of star formation. Therefore, measurements of H I mass loss are needed to test theoretical predictions. Models of galaxy evolution predict a decline in the mass-loss efficiency such that $\dot{M}_{out}/SFR \propto M_{star}^{-1/2}$ (Pandya et al., 2021). Currently, the observations used to constrain this are of ionised gas, which do not carry the largest component of mass. We do not know if the relative mass-loss of H I to ionised gas changes with galaxy mass, star formation rate or other properties such as metallicity. At lower masses, starburst galaxies are more metal-poor and more highly ionised which may impact the details of the multiphase outflows. Moreover, it is not clear how the mass-loading of H I changes for AGNs and star formation feedback. Because, AGN feedback becomes more important at larger masses, this must be understood to generate full models of galaxy evolution. Surveys of sufficient numbers of outflows are needed to apply this constraint to galaxy evolution.

### 2.2 What SKA can add to mass-loss from outflows

There is an urgent need for a systematic survey to target outflows in cold gas across a range of galaxy stellar masses. Due to the limits to sensitivity, as well as decreasing brightness of CO for low metallicity galaxies, ALMA is unlikely to achieve this. Because galactic winds are rare, observations must probe beyond the nearest galaxies. Both resolution and sensitivity become critical parameters that require sufficient recovery of outflow flux, with robust seperation of the outflow from the galaxy. SKA-mid AA* will provide kiloparsec-scale resolution at 1.4GHz and reach the required sensitivity in 10hr integration with a 10 arcsec beam. This provides sufficient detections of $\sim 2-5\times10^{19}$ cm$^{-2}$, comparable to other outflow measurements (e.g. Martini et al., 2018). Using such data one could robustly probe outflows in galaxies $\sim$ 50 Mpc away, sufficient to build samples of ~10 outflow galaxies per 0.5 dex bins in stellar mass (McQuinn et al., 2019; Marasco et al., 2023; van de Sande et al., 2023).

At 50 Mpc the 10 arcsec beam has a physical size of ~2.5 kpc. Recently, Mazzilli Ciraulo et al. (2025) combined ASKAP-WALLABY observations (Lee et al., 2022) with VLT/MUSE and narrow-band H$\alpha$ observations of the outflow in nearby galaxy NGC 4666. The galaxy is nearby, $d \sim 15.5$ Mpc, and the WALLABY beam corresponds to ~2.5 kpc in this galaxy. Moreover, WALLABY is a relatively shallow, wide area survey. These observations, therefore, demonstrate that even with coarse spatial sampling outflows can be measured at this resolution. As can be seen in Fig. 5 the H I distribution above and below the disk follows the orientation of the H$\alpha$ filaments associated with the outflow. Moreover, the velocity offsets shown in Fig. 5 also increase in the outflow region (beyond $\sim$ 4 kpc), both for H I and the ionised gas. This galaxy represents the third strong outflow system where we can resolve H I mass-loss due to the wind. This demonstrates the limits of what can be done with H I observations of very nearby targets. SKA AA* will push this forward significantly.

### 2.3 Galactic fountain regulation of mass growth in Milky Way-like disk galaxies

The regulation of stellar mass growth by star formation feedback remains a dominant feature of galaxies with more modest star formation rates. Spiral galaxies are understood to maintain an equilibrium in which feedback from young stars and supernovae determines the star formation rate

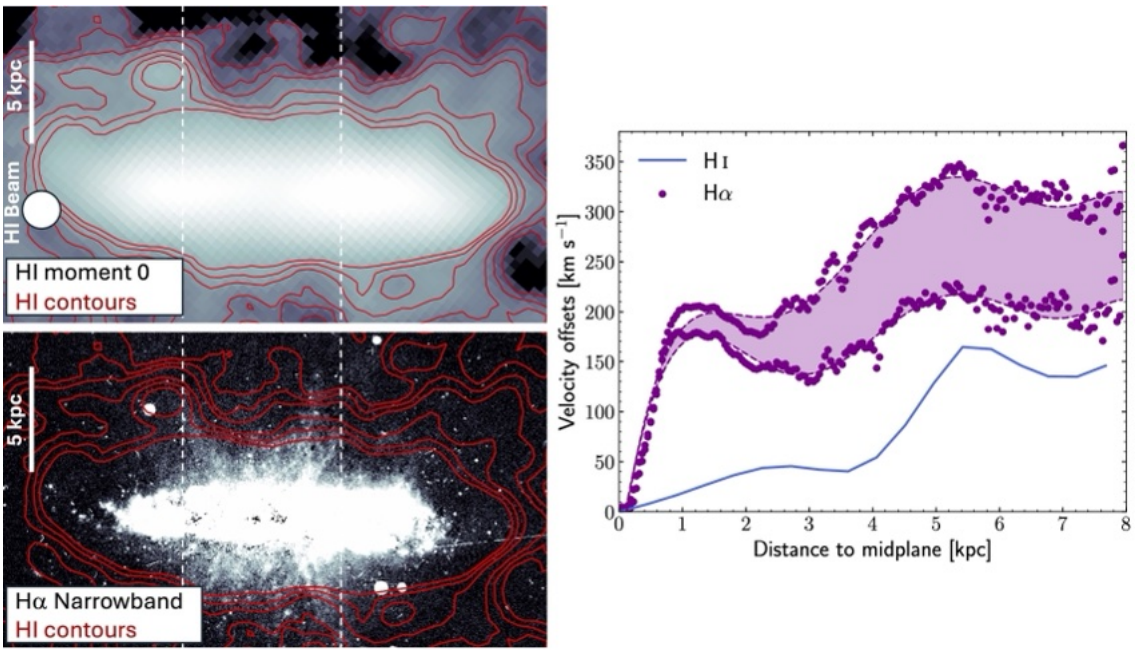


**Figure 5:** H I moment 0 map of the outflow in NGC 4666 is compared to H$\alpha$ map of the same target. The biconical outflow is evident at higher spatial resolution, and H I contours show a response to the outflow. Using current facilities this can be achieved only on the nearest targets ($\lesssim$15 Mpc), and requires prohibitively long exposures with MeerKAT or VLA.

of the galaxy (Ostriker and Shetty, 2011). The feedback acts in multiple ways. The injection of energy and momentum in to the ISM generates turbulence, which thickens the disk and reduces star formation. Kinematic observations of both H I and CO support this picture in local Universe galaxies (Bacchini et al., 2020; Girard et al., 2021; Lenkić et al., 2024).

At the same time, energy from supernova also drives gas vertically out of the disk plane, often described as a superbubble (Mac Low et al., 1989). Superbubbles cool as they expand. The initially hot gas from the disk rains back down as cool neutral gas in a so-called “galactic fountain" (Shapiro and Field, 1976). This process slows star formation in the disk by moving gas into the inner-circumgalactic medium, where it will not form stars. Moreover, cold gas may be entrained in the superbubble as it is launched, which very directly reduces the gas mass available for star formation.

NGC 891 provides one of the best examples of cold gas in galactic fountains. Oosterloo et al. (2007b) show a filament extending ~20 kpc into the circumgalactic medium, upward from the midplane of the disk. The mass of the filament is of order $\sim 10^9$ M$_\odot$, and is more massive than associated X-ray gas. This suggests that cold gas likewise dominates the ejected mass in lower amplitude galactic fountains, which may be a universal feature of all outflowing gas including both large-scale biconical outflows and smaller galactic fountains. Indeed, the cold gas dominates the outflowing mass even at very low altitudes above the disk plane, which suggests that cold gas entrainment may be a critical feature of galactic fountains (e.g. Hodges-Kluck and Bregman, 2013).

Recent deep imaging with the FAST 500 m single dish telescope shows vast reservoirs of H I gas surrounding disk galaxies, including NGC 891 (Yang et al., 2025). These reservoirs strongly suggest a mechanism to maintain them. Moreover, when gas moves out of the plane of disks into the halo, it does not enter into a void of empty space. Cooling of hot halo gas is made much more efficient by the mixing of metal-rich gas from feedback driven winds with existing halo gas (Armillotta et al., 2016), which then will impact the rate of accretion onto the galaxy. The extraplanar gas above a star forming galaxies is, therefore, a mixture of feedback driven winds (and fountains) and accretion onto galaxies (described above). A full characterisation of both processes is necessary to understand the mass growth in galaxies (see review Fraternali, 2017).

Signatures of these processes are found in the kinematics of disk galaxies. "Lagging" rotation velocity above the plane of the disk has been observed for many years, with the most significant sample (Marasco et al., 2019) using the HALOGAS survey. They modelled extraplanar H I gas in 15 galaxies, and found this thick layer is nearly ubiquitous, and is consistent with models in which this thick layer is fed by the mixture of gas driven to large heights by feedback and gas that is cooling from the halo. Recent work with MeerKAT (Ianjamasimanana et al., 2022) shows similar thick layers of H I around edge-on disk galaxies.

It is natural to expect this process to vary with the strength of the starburst. Higher gas density in the disk generates larger, higher density star clusters (reviews Krumholz et al., 2019; Schinnerer and Leroy, 2024). More massive star clusters naturally generate more supernovae, and thus generate larger superbubbles. What remains very unclear is the amount of cold gas that couples to this feedback, and how far it travels from the disk. High resolution simulations of these processes have significant problems reproducing the cold gas seen in strong winds (Rathjen et al., 2021; Kim et al., 2017). Direct comparison to systematic studies at star formation rates more similar to Milky Way remain out of reach of current observatories.

### 2.4 What SKA adds to our understanding of galactic fountain driven baryon cycle

Similar to observations of winds, observing galactic fountains requires a combination of fine spatial resolution and deep sensitivity. While galaxies with galactic fountain-style gas flows are far more common than strong starburst galaxies the resultant superbubbles are smaller, and thus require finer spatial resolution to identify and measure.

Superbubbles have historically been observed as holes of H I gas in face-on galaxies (e.g. Boomsma et al., 2008). Because the pressure is decreasing more rapidly in the vertical direction we expect superbubbles to extend $\sim 3-5\times$ further vertically than in the plane of the disk. Statistical analysis of large samples of bubbles in high-spatial resolution JWST imaging of PAH emission (Watkins et al., 2023) suggests that sub-kpc spatial resolution is needed for direct imaging of individual bubbles. It is not clear what sensitivity is needed for the extraplanar component of H I in bubbles. In the disk, H I holes have a high-surface density, though we expect the z-axis component to be less. The highest resolution achievable would allow for characterization of bubbles with diameter ~200-300 pc in galaxy at a distance 10-15 Mpc. This allows for substructure of the bubble. If fainter observations are necessary, then $\sim 1-5\times10^{19}$ cm$^{-2}$ at sub-kpc resolution can still be achieved with 10 hr observations of SKA AA*, for galaxies that are nearer than $\sim$ 15 Mpc. Theories of feedback

make direct predictions for the evolution of a superbubble in comparison to the energy derived from star formation rate. Using SKA H I observations, one can determine the size, and kinematics of the bubble. This can then be directly compared to SFR of the driver, with radio continuum or another tracer. If bubbles have systematically different sizes and kinematics compared to theory, then modifications to feedback theory are needed.

## 3 Mass accretion from observations of the Milky Way and the Local Group galaxies

### 3.1 Galaxy Evolution and the Gas Depletion Problem

As already mentioned in the previous sections, galaxies form within dark matter haloes that grow hierarchically in the ΛCDM cosmology (White and Rees, 1978), and their primary mass supply is maintained by the smooth accretion of cold gas along the cosmic filaments (Kereš et al., 2005; Dekel et al., 2009). In the present-day universe, mass accretion onto galaxies is no longer considered the dominant driving mechanism of their growth; instead, mergers are thought to be the primary mode. Galaxy evolution is driven by star formation and its feedback, with the interstellar medium (ISM) serving as the fuel for this process. The currently observed star formation rate in the Milky Way, estimated from infrared satellite observations, is on the order of a few solar masses per year, while the gas mass presently contained is about $10^9$ $M_\odot$. If the star formation rate remains at its current level, it has been pointed out that the gas would be depleted within less than about one billion years. Against this background of the so-called "gas depletion problem," in this section, we introduce recent studies within the Milky Way on H I gas clouds falling onto the Galactic disk, and review the impact of mass accretion on star formation in nearby galaxies within the Local Group. We then propose an observational study using H I observations of external galaxies with the SKA to place constraints on the mode of galaxy evolution in the present-day universe, particularly through quantitative measurements of mass accretion.

### 3.2 Observations of Extraplanar Gas in the Milky Way

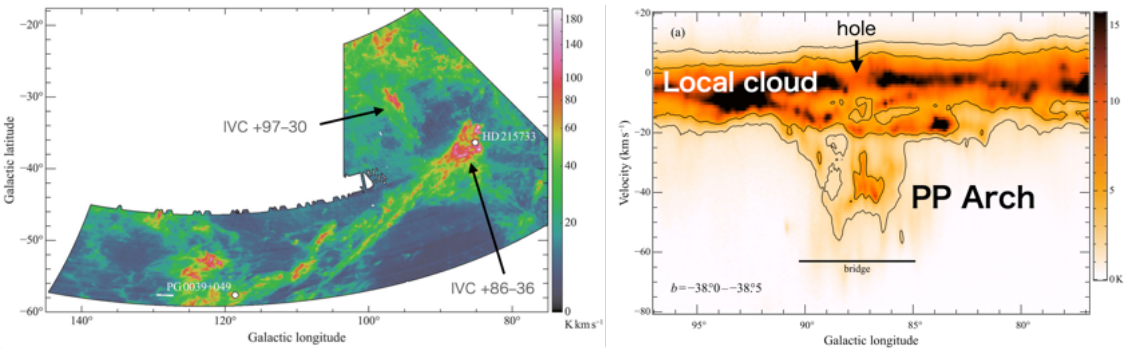


**Figure 6:** Left: Integrated H I intensity map of the IVC "PP Arch" identified from HI4PI data. A characteristic head–tail morphology is evident. Right: Longitude–velocity diagram around the head region of the PP Arch. The IVC shows a blue-shift of about 40 km s$^{-1}$ relative to the nearby local cloud at ~ 0 km s$^{-1}$, and a diffuse bridge structure connects the two. A cavity is also seen in the local cloud, likely formed as a result of the interaction between them. Modified from Fukui et al. (2021).

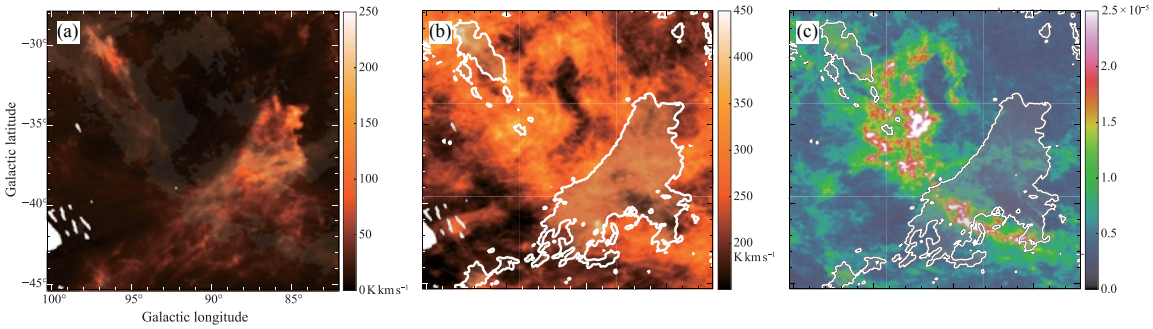


**Figure 7:** (a) Integrated H I intensity map of the head region of the PP Arch for velocities between −60 and −30 km s$^{-1}$. Two IVCs, IVC +86–36 and IVC +97–30, are seen. (b) The same region integrated over −30 to +30 km s$^{-1}$, showing the nearby local cloud. Contours indicate the IVCs from panel (a). (c) Distribution of dust optical depth $\tau_{353}$ in the same region. Contours again trace the IVCs from panel (a). The high-latitude local cloud corresponds to the MBM 53–55 complex, while no significant dust emission is associated with IVC +86–36. Modified from Fukui et al. (2021).

H I 21-cm line observations have revealed the presence of High Velocity Clouds (HVCs) and Intermediate Velocity Clouds (IVCs) in the Milky Way. HVCs are clouds moving with velocities deviating by more than 100 km s$^{-1}$ from the Galactic rotation, most of which exhibit negative line-of-sight velocities. In contrast, IVCs have velocities of about 30–90 km s$^{-1}$, and both are thought to be falling toward the Galactic plane. HVCs are generally interpreted as clouds accreting from the Galactic halo onto the disk, while IVCs have traditionally been explained by the "Galactic fountain" model, in which gas circulates within the Milky Way (Wakker, 2004). This interpretation was primarily based on metallicity measurements from absorption lines: HVCs are composed of low-metallicity gas, whereas IVCs are thought to be metal-rich. However, recent measurements of elemental abundances have shown that the metallicities of IVCs are not as high as previously believed, suggesting that IVCs may have intermediate properties between typical HVCs and local clouds.

These studies have been enabled by all-sky surveys of the H I 21-cm line and submillimeter dust continuum emission. Fukui et al. (2021) investigated an H I IVC with a characteristic head–tail morphology, known as the PP Arch (Figure 6). They first found that a remarkable feature of this cloud is its extremely faint dust continuum emission (Figure 7). In sharp contrast to the nearby high-latitude cloud complex MBM 53–55, the PP Arch exhibits a dust-to-gas ratio that is estimated to be significantly smaller by a factor of several to an order of magnitude compared with typical local interstellar clouds. The morphology of a dense head followed by a narrow, trailing tail has been well reproduced by numerical simulations (Shelton et al., 2022). These simulations suggest that an H I cloud falling from a height of ∼,a few hundred parsecs above the Galactic disk interacts with the surrounding medium as it approaches the disk, gradually decelerating through ram pressure drag and mixing with the local gas. Indeed, in the PP Arch, clear signatures of interaction are observed between the IVC and the local gas that follows the Galactic rotation.

The dust-to-gas ratio was measured by dividing the cloud into spatial meshes and calculating the ratio between the H I integrated intensity and the dust optical depth (Fig. 8). The dust optical depth

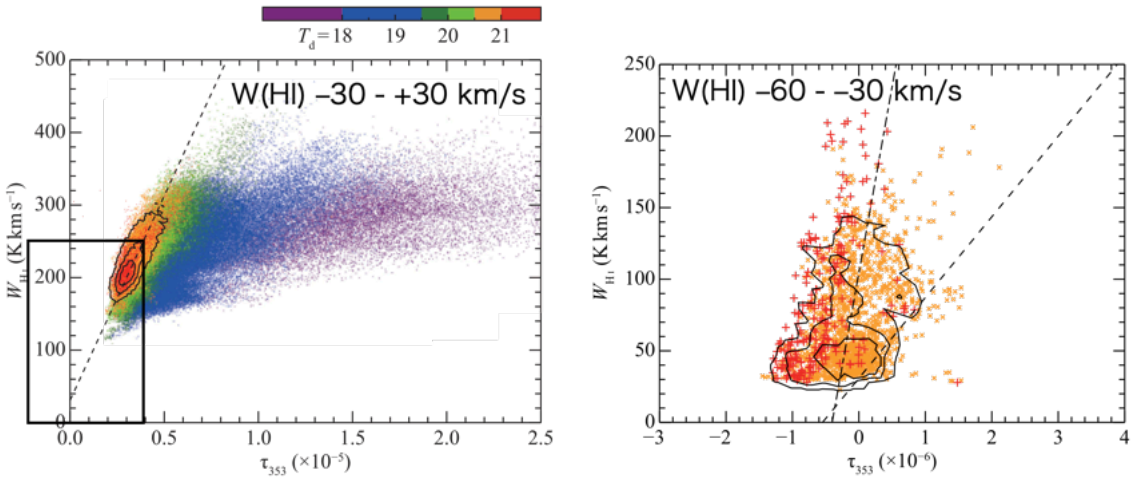


**Figure 8:** Correlation plots between the integrated H I intensity $W$(HI) and the dust optical depth $\tau_{353}$ for the region shown in Figure 7. The left panel corresponds to the velocity range −30 to +30 km s$^{-1}$ for the local cloud, while the right panel corresponds to the velocity range −60 to −30 km s$^{-1}$ for the IVC. The square in the left panel indicates the plotting range of the right panel. The dashed line represents the best-fit relation between $W$(H I ) and $\tau_{353}$ derived for optically thin H I in the local cloud, which has a relatively high dust temperature. The dash–dotted line in the right panel shows the best-fit relation for the IVC velocity range. The slopes of these lines represent the dust-to-gas ratio. Modified from Fukui et al. (2021).

was derived from spectral energy distribution (SED) fitting to multi-band continuum data obtained by the Planck satellite. This approach represented a major improvement over previous methods, which relied solely on absorption-line measurements toward discrete background sources, allowing for the first time a two-dimensional map of the dust-to-gas ratio distribution (see also Fukui et al., 2014, 2015; Okamoto et al., 2017). In the case of IVC +86–36, absorption-line spectroscopy toward the background star HD 215733 yielded a subsolar elemental abundance. However, the measurement suffers from large uncertainties due to ionization effects and elemental depletion onto dust grains, as well as the fact that it represents only a single line of sight.

Building on these results, Hayakawa and Fukui (2024) extended the same analysis to the entire sky excluding the Galactic plane. Figure 9 shows the distribution of IVCs in one quarter of the northern Galactic hemisphere, revealing that a significant fraction of the clouds exhibit relatively low metallicities. The distribution of IVC metallicities (Fig. 10) demonstrates that they possess intermediate properties between those of HVCs and local clouds. This finding challenges the traditional Galactic fountain scenario—in which material is expelled from the Galactic disk, cools, and subsequently falls back—and instead supports the interpretation proposed from the PP Arch observations: that IVCs represent decelerated HVCs that have mixed with the more metal-rich interstellar medium near the Galactic plane. If this interpretation is correct, the IVCs currently observed in the Milky Way are expected to lie relatively close to the Galactic disk. Therefore, estimating their total mass across the entire Galaxy remains difficult. Nevertheless, if the inflow rate of low-metallicity hydrogen gas accreting from the Galactic halo is on the order of a few $M_\odot$ yr$^{-1}$, it would be sufficient to sustain the ongoing star formation in the Milky Way. Conversely, if the actual accretion rate is significantly lower, the interstellar gas in the Galaxy would be depleted

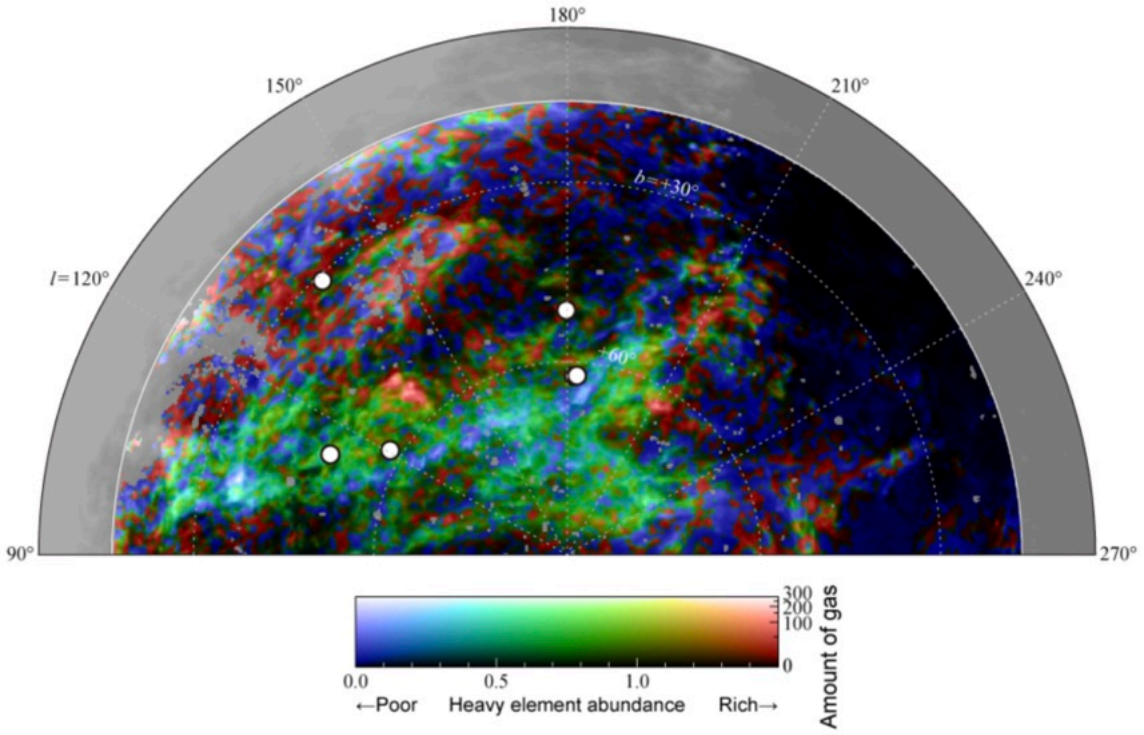


**Figure 9:** Distribution of IVCs in the northern Galactic hemisphere ($b > 0°$), covering Galactic longitudes 90°–270°. Colors indicate the relative metallicity of the interstellar medium, with blue representing metal-poor and red representing metal-rich gas. White circles mark the positions of background sources toward which absorption-line measurements have been obtained. Modified from Hayakawa and Fukui (2024).

on a timescale of about one billion years, leading to the eventual cessation of star formation. In this context, the presence of external gas accretion in the current and future Milky Way is of critical importance, and constraining the mass accretion rate provides a key to predicting the Galaxy's future evolution.

In recent years, CO line observations have also revealed molecular clouds that appear to be infalling toward the Galactic disk. Kohno et al. (2025) identified a molecular cloud with a head–tail morphology extending vertically from the Galactic plane. Multi-$J$ CO line observations show that the CO (2–1)/(1–0) line intensity ratio is enhanced in the head region, and LVG analysis indicates that the kinetic temperature ($T_{\rm kin}$) rises above 40 K. Since there is no evidence of associated star formation, this heating is interpreted as shock heating caused by the collision of the infalling cloud with the Galactic disk. Although it is observationally difficult to directly determine the vertical ($Z$-direction) motion of molecular clouds near the Galactic plane, if the motion originates from infalling H I gas, it implies that both mass and kinetic energy are being supplied from the Galactic halo to the giant molecular clouds (GMCs) in the disk.

Through tidal interactions with the Milky Way, gas has been stripped from the Large and Small Magellanic Clouds, forming the Magellanic Stream (MS), which extends over more than 100 degrees across the sky. The stream is observed as a HVCs system in H I 21 cm emission (Putman et al.,

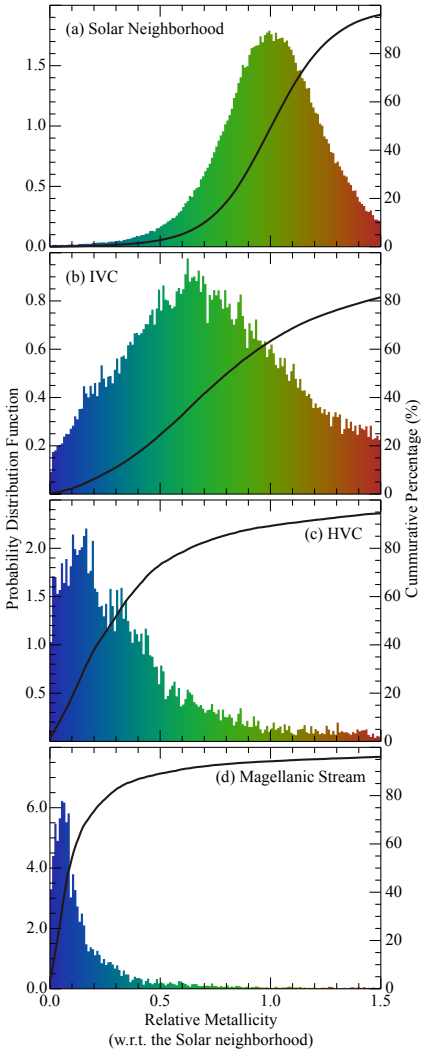


**Figure 10:** Histograms of the relative dust-to-gas ratio with respect to the average value of local clouds near the Sun, for (a) local clouds, (b) IVCs, (c) HVCs, and (d) the Magellanic Stream. Modified from Hayakawa and Fukui (2024).

1998; Brüns et al., 2005). Its total mass is estimated to be about $1.6 \times 10^8$, $M_\odot$ (Brüns et al., 2005). In comparison, the total mass of all HVCs is estimated to be $\sim 2.5 \times 10^8$, $M_\odot$ (Wakker, 2004), indicating that roughly half of the HVC population originates from the MS. As shown in Figure 10, the metallicity of the MS is as low as about 0.1 solar, suggesting an origin in the Small Magellanic Cloud (SMC). By contrast, the metallicity of other HVCs is significantly higher than that of the MS. This implies that the HVCs have undergone substantial metal enrichment, possibly through mixing with interstellar material (ISM) lifted to high altitudes by the galactic fountain, or through interactions with the ISM near the Galactic disk after infall, while still retaining high velocities.

Fox et al. (2014) estimated the mass accretion rate due to the infall of the MS to be about 2, $M_\odot$, $\mathrm{yr}^{-1}$. In contrast, Richter et al. (2017) estimated a total accretion rate of $\sim 6.1$, $M_\odot$, $\mathrm{yr}^{-1}$ when including

both neutral and ionized gas from all HVCs, including the MS. This rate is sufficient to sustain, or even exceed, the current star formation rate of the Milky Way. However, considering the present total mass of the HVC system, such gas would be depleted within roughly $10^8$ years. To compensate for this depletion, either additional tidal stripping of gas from nearby satellite galaxies or the cooling and subsequent infall of hot, ionized coronal gas in the Galactic halo would be required.

### 3.3 Proposed Observations of Accreting Gas in Nearby Galaxies

Gas exchange is frequently observed between interacting galaxies in the nearby universe. The most prominent example is the Large and Small Magellanic Clouds, whose connecting structure, the Magellanic Bridge (MB), is thought to have formed as a result of tidal interactions. This process has been successfully reproduced by many numerical simulations (e.g., Murai and Fujimoto, 1980), and Gaia observations have revealed stellar motions from the SMC toward the LMC (Schmidt et al., 2020). At the same time, observations have shown that the tidal forces are severely stretching and disrupting the less massive SMC (Nakano et al., 2025; Nakano and Tachihara, 2025). As a consequence of this tidal interaction, it has been suggested that gas accretion from the SMC onto the LMC triggered active star formation observed for example in 30 Doradus through its collision with the LMC disk (Fukui et al., 2017; Tsuge et al., 2019, 2024). Similar mass exchange has been proposed for the M31–M33 system, where active star formation in NGC 604 may have been induced by such an interaction (Tachihara et al., 2018). These phenomena are thought to be driven by high-velocity gas collisions of up to $\sim$ 100 km s$^{-1}$, which efficiently compress and densify the H I gas. Signs of comparable intergalactic interactions have been observed in many other interacting systems. For example, the MHONGOOSE project with MeerKAT detected nine satellite galaxies around the edge-on galaxy UGCA 250, revealing a tail-like H I structure extending toward one of them (Kurapati et al., 2025). See previous sections for more details about the MHONGOOSE project.

Comparable investigations can also be applied to galaxies that do not exhibit clear evidence of tidal interaction. In particular, for evolved disk galaxies, if cooling of hot ionized coronal gas or intergalactic gas can be directly observed as it condenses and falls toward the disk as HVCs, it would enable estimates of the quasi-steady mass accretion rate onto the galaxy. Observations of edge-on galaxies are especially effective for this purpose. By detecting extraplanar H I gas located above the galactic plane and separating it from the rotating disk component, one can identify accreting structures. Following the approach used in the Milky Way, correlations between H I and dust emission should then be examined. Dust emission from such high-altitude extraplanar gas can be effectively traced by submillimeter continuum observations with ALMA. By measuring the metallicity of the extraplanar gas relative to that of the galactic disk, it becomes possible to distinguish whether the HVCs originate from galactic fountain processes or from infalling halo gas, thereby constraining the external mass accretion rate. Conducting such studies for a large sample of nearby galaxies—particularly for evolved disk systems—will enable a statistical investigation of present-day galactic gas dynamics and provide insights into the future evolution of mature galaxies.

Previous observations from projects like VLA THINGS (Walter et al., 2008), ATCA LVHIS (Koribalski et al., 2018), and WSRT HALOGAS (e.g., Marasco et al. 2019) have achieved resolutions of about 7″–30″. MeerKAT MHONGOOSE has observed nearby galaxies with 8″ resolution.

SKA AA4 will achieve higher spatial resolution and sensitivities. With a resolution of 6″ (300 pc at the distance of 10 Mpc), an H I column density sensitivity of $N_{\rm HI} \sim$ a few $\times 10^{18}$ cm$^{-2}$ is expected, enabling the detection of H I clouds of a few $\times 10^3$ $M_\odot$. The UNGC/LVG database catalogs 869 galaxies within 11 Mpc (Karachentsev et al., 2013). Among these, disk galaxies comprise approximately 20%. Estimating the number of edge-on galaxies with an axial ratio $\lesssim 0.25$, i.e., $i > 80°$, yields roughly 20 such galaxies. Galaxies showing no obvious signs of interaction, such as UGC 7321, ESO 274-G001, and IC 5052, are good candidates for isolated galaxies. On the other hand, there are also clear interacting galaxies, such as NGC 3628 with its long tidal tail. Comparative studies of these will investigate the effects of perturbations from nearby galaxies on mass accretion. Through the statistical studies of many galaxies by SKA AA4, our understanding of mass accretion into evolved disk galaxies will advance dramatically, and additionally will provide clues about the future evolution of the Milky Way Galaxy.

**Acknowledgements**
This work has received funding from the European Research Council (ERC) under the European Union's Horizon 2020 research and innovation programme (grant agreement No. 882793 "MeerGas"). FMM carried out part of the research activities described in this paper with contribution of the Next Generation EU funds within the National Recovery and Resilience Plan (PNRR), Mission 4 - Education and Research, Component 2 - From Research to Business (M4C2), Investment Line 3.1 - Strengthening and creation of Research Infrastructures, Project IR0000034 – "STILES - Strengthening the Italian Leadership in ELT and SKA". LC acknowledges financial support from the French Agence Nationale de la Recherche ANR.

## References

L. Armillotta, F. Fraternali, and F. Marinacci. *MNRAS*, 462(4):4157–4170, Nov. 2016. doi: 10.1093/mnras/stw1930.
R. Auld, R. F. Minchin, J. I. Davies, et al. *MNRAS*, 371(4):1617, 2006.
C. Bacchini et al. *A&A*, 641:A70, Sept. 2020. doi: 10.1051/0004-6361/202038223.
I. Bagetakos, E. Brinks, F. Walter, et al. *AJ*, 141:23, 2011.
D. G. Barnes, L. Staveley-Smith, W. J. G. de Blok, et al. *MNRAS*, 322(3):486, 2001.
A. D. Bolatto et al. *Nature*, 499(7459):450–453, July 2013. doi: 10.1038/nature12351.
R. Boomsma et al. *A&A*, 490(2):555–570, Nov. 2008. doi: 10.1051/0004-6361:200810120.
J. N. Bregman. *ApJ*, 236:577, 1980.
C. Brüns et al. *A&A*, 432(1):45–67, Mar. 2005. doi: 10.1051/0004-6361:20040321.
W. J. G. de Blok, J. Healy, F. M. Maccagni, et al. *A&A*, 688:A109, 2024.
A. Dekel et al. *Nature*, 457(7228):451–454, Jan. 2009. doi: 10.1038/nature07648.
N. M. Förster Schreiber and S. Wuyts. *ARA&A*, 58:661–725, Aug. 2020. doi: 10.1146/annurev-astro-032620-021910.
A. J. Fox et al. *ApJ*, 787(2):147, June 2014. doi: 10.1088/0004-637X/787/2/147.
F. Fraternali. In *IAU Symposium*, volume 298, 2013.
F. Fraternali. In A. Fox and R. Davé, editors, *Gas Accretion onto Galaxies*, volume 430 of *Astrophysics and Space Science Library*, page 323, Jan. 2017. doi: 10.1007/978-3-319-52512-9_14.

Y. Fukui et al. *ApJ*, 796(1):59, Nov. 2014. doi: 10.1088/0004-637X/796/1/59.
Y. Fukui et al. *ApJ*, 798(1):6, Jan. 2015. doi: 10.1088/0004-637X/798/1/6.
Y. Fukui et al. *PASJ*, 69(3):L5, June 2017. doi: 10.1093/pasj/psx032.
Y. Fukui et al. *PASJ*, 73:S117–S128, Jan. 2021. doi: 10.1093/pasj/psy120.
M. Girard et al. *ApJ*, 909(1):12, Mar. 2021. doi: 10.3847/1538-4357/abd5b9.
T. Hayakawa and Y. Fukui. *MNRAS*, 529(1):1–31, Mar. 2024. doi: 10.1093/mnras/stae302.
M. P. Haynes, R. Giovanelli, B. R. Kent, et al. *ApJ*, 861(1):49, 2018.
G. Heald, G. Józsa, P. Serra, et al. *A&A*, 526:A118, 2011.
E. J. Hodges-Kluck and J. N. Bregman. *ApJ*, 762(1):12, Jan. 2013. doi: 10.1088/0004-637X/762/1/12.
D. A. Hunter, D. Ficut-Vicas, T. Ashley, et al. *AJ*, 144:134, 2012.
R. Ianjamasimanana, W. J. G. de Blok, and G. H. Heald. *AJ*, 153(5):213, 2017.
R. Ianjamasimanana et al. *MNRAS*, 513(2):2019–2038, June 2022. doi: 10.1093/mnras/stac936.
J. A. Irwin, G. L. Hoffman, K. Spekkens, et al. *ApJ*, 692:1447, 2009.
M. Johnson et al. *AJ*, 144(5):152, Nov. 2012. doi: 10.1088/0004-6256/144/5/152.
I. D. Karachentsev, D. I. Makarov, and E. I. Kaisina. *AJ*, 145(4):101, Apr. 2013. doi: 10.1088/0004-6256/145/4/101.
D. Kereš, N. Katz, D. H. Weinberg, and R. Davé. *MNRAS*, 363(2), 2005.
D. Kereš, N. Katz, D. H. Weinberg, and R. Davé. *MNRAS*, 363(1):2–28, Oct. 2005. doi: 10.1111/j.1365-2966.2005.09451.x.
C.-G. Kim, E. C. Ostriker, and R. Raileanu. *ApJ*, 834:25, Jan. 2017. doi: 10.3847/1538-4357/834/1/25.
M. Kohno et al. *arXiv e-prints*, art. arXiv:2510.18399, Oct. 2025. doi: 10.48550/arXiv.2510.18399.
B. S. Koribalski et al. *MNRAS*, 478(2):1611–1648, Aug. 2018. doi: 10.1093/mnras/sty479.
B. S. Koribalski, J. Wang, P. Kamphuis, et al. *MNRAS*, 478(2):1611, 2018.
B. S. Koribalski, L. Staveley-Smith, T. Westmeier, et al. *Ap&SS*, 365(7):118, 2020.
M. R. Krumholz, C. F. McKee, and J. Bland-Hawthorn. *ARA&A*, 57:227–303, Aug. 2019. doi: 10.1146/annurev-astro-091918-104430.
S. Kurapati et al. *MNRAS*, 538(2):1272–1287, Apr. 2025. doi: 10.1093/mnras/staf387.
B. Lee et al. *ApJS*, 262(1):31, Sept. 2022. doi: 10.3847/1538-4365/ac7eba.
L. Lenkić et al. *ApJ*, 976(1):88, Nov. 2024. doi: 10.3847/1538-4357/ad758c.
A. K. Leroy et al. *ApJ*, 814(2):83, Dec. 2015. doi: 10.1088/0004-637X/814/2/83.
M.-M. Mac Low, R. McCray, and M. L. Norman. *ApJ*, 337:141, Feb. 1989. doi: 10.1086/167094.
F. M. Maccagni and W. J. G. de Blok. *arXiv preprint*, 2024. doi: 10.48550/arXiv.2407.03166.
A. Marasco et al. *A&A*, 631:A50, Nov. 2019. doi: 10.1051/0004-6361/201936338.
A. Marasco et al. *A&A*, 670:A92, Feb. 2023. doi: 10.1051/0004-6361/202244895.
A. Marasco, W. J. G. de Blok, F. M. Maccagni, et al. *A&A*, 697:A86, 2025.
P. Martini et al. *ApJ*, 856(1):61, Mar. 2018. doi: 10.3847/1538-4357/aab08e.
B. Mazzilli Ciraulo et al. *arXiv e-prints*, art. arXiv:2509.17560, Sept. 2025. doi: 10.48550/arXiv.2509.17560.
K. B. W. McQuinn, L. van Zee, and E. D. Skillman. *ApJ*, 886(1):74, Nov. 2019. doi: 10.3847/1538-4357/ab4c37.
M. J. Meyer, M. A. Zwaan, R. L. Webster, et al. *MNRAS*, 350(4):1195, 2004.

T. Murai and M. Fujimoto. *PASJ*, 32(4):581–603, Dec. 1980. doi: 10.1093/pasj/32.4.581.
S. Nakano and K. Tachihara. *ApJL*, 985(1):L5, May 2025. doi: 10.3847/2041-8213/adce0b.
S. Nakano, K. Tachihara, and M. Tamashiro. *ApJS*, 277(2):62, Apr. 2025. doi: 10.3847/1538-4365/adb8de.
D. Nelson et al. *MNRAS*, 490(3):3234–3261, Dec. 2019. doi: 10.1093/mnras/stz2306.
C. A. Norman and S. Ikeuchi. *ApJ*, 345:372, 1989.
R. Okamoto et al. *ApJ*, 838(2):132, Apr. 2017. doi: 10.3847/1538-4357/aa6747.
T. Oosterloo, F. Fraternali, and R. Sancisi. *AJ*, 134(3):1019, Sept. 2007a. doi: 10.1086/520332.
T. Oosterloo, F. Fraternali, and R. Sancisi. *AJ*, 134(3):1019, Sept. 2007b. doi: 10.1086/520332.
E. C. Ostriker and R. Shetty. *ApJ*, 731:41, Apr. 2011. doi: 10.1088/0004-637X/731/1/41.
V. Pandya et al. *MNRAS*, 508(2):2979–3008, Dec. 2021. doi: 10.1093/mnras/stab2714.
A. Pillepich et al. *MNRAS*, 473(3):4077–4106, Jan. 2018. doi: 10.1093/mnras/stx2656.
N. M. Pingel, D. J. Pisano, G. Heald, et al. *ApJ*, 865(1):36, 2018.
M. E. Putman et al. *Nature*, 394(6695):752–754, Aug. 1998. doi: 10.1038/29466.
M. E. Putman, J. E. G. Peek, and M. R. Joung. *ARA&A*, 50:491, 2012.
T.-E. Rathjen et al. *MNRAS*, 504(1):1039–1061, June 2021. doi: 10.1093/mnras/stab900.
B. Reichardt Chu et al. *MNRAS*, 536(2):1799–1821, Jan. 2025. doi: 10.1093/mnras/stae2705.
P. Richter et al. *A&A*, 607:A48, Nov. 2017. doi: 10.1051/0004-6361/201630081.
R. Sancisi, F. Fraternali, T. Oosterloo, and T. van der Hulst. *A&A Review*, 15:189, 2008.
A. Sardone, D. J. Pisano, N. M. Pingel, et al. *ApJ*, 910(1):69, 2021.
E. Schinnerer and A. K. Leroy. *ARA&A*, 62(1):369–436, Sept. 2024. doi: 10.1146/annurev-astro-071221-052651.
T. Schmidt et al. *A&A*, 641:A134, Sept. 2020. doi: 10.1051/0004-6361/202037478.
P. R. Shapiro and G. B. Field. *ApJ*, 205:762–765, May 1976. doi: 10.1086/154332.
P. R. Shapiro and G. B. Field. *ApJ*, 205:762, 1976.
R. L. Shelton et al. *ApJ*, 925(2):190, Feb. 2022. doi: 10.3847/1538-4357/ac39a4.
A. Sorgho, C. Carignan, D. J. Pisano, et al. *MNRAS*, 482(1):1248, 2019.
K. Tachihara et al. *PASJ*, 70:S52, May 2018. doi: 10.1093/pasj/psy020.
T. A. Thompson and T. M. Heckman. *ARA&A*, 62(1):529–591, Sept. 2024. doi: 10.1146/annurev-astro-041224-011924.
K. Tsuge et al. *ApJ*, 871(1):44, Jan. 2019. doi: 10.3847/1538-4357/aaf4fb.
K. Tsuge et al. *PASJ*, 76(4):589–615, Aug. 2024. doi: 10.1093/pasj/psae035.
J. Tumlinson, M. S. Peeples, and J. K. Werk. *ARA&A*, 55(1):389–432, Aug. 2017. doi: 10.1146/annurev-astro-091916-055240.
J. van de Sande et al. *arXiv e-prints*, art. arXiv:2306.00059, May 2023. doi: 10.48550/arXiv.2306.00059.
J. M. van der Hulst, T. S. van Albada, and R. Sancisi. In *ASP Conference Series*, volume 240, page 451, 2001.
S. Veilleux, G. Cecil, and J. Bland-Hawthorn. *ARA&A*, 43(1):769–826, Sept. 2005. doi: 10.1146/annurev.astro.43.072103.150610.
S. Veilleux, R. Maiolino, A. D. Bolatto, and S. Aalto. *A&ARv*, 28(1):2, Apr. 2020. doi: 10.1007/s00159-019-0121-9.
B. P. Wakker. In H. van Woerden, B. P. Wakker, U. J. Schwarz, and K. S. de Boer, editors, *High*

*Velocity Clouds*, volume 312 of *Astrophysics and Space Science Library*, page 25, Jan. 2004. doi: 10.1007/1-4020-2579-3_2.

F. Walter et al. *AJ*, 136(6):2563–2647, Dec. 2008. doi: 10.1088/0004-6256/136/6/2563.

F. Walter, E. Brinks, W. J. G. de Blok, et al. *AJ*, 136:2563, 2008.

J. Wang et al. *ApJ*, 968(1):48, June 2024. doi: 10.3847/1538-4357/ad3e61.

E. J. Watkins et al. *A&A*, 676:A67, Aug. 2023. doi: 10.1051/0004-6361/202346075.

S. D. M. White and M. J. Rees. *MNRAS*, 183:341–358, May 1978. doi: 10.1093/mnras/183.3.341.

S. A. Wolfe, F. J. Lockman, and D. J. Pisano. *ApJ*, 816(2):81, 2016.

R. J. Wright et al. *MNRAS*, 532(3):3417–3440, Aug. 2024. doi: 10.1093/mnras/stae1688.

X. Xu et al. *ApJ*, 956(2):142, Oct. 2023. doi: 10.3847/1538-4357/acfa71.

D. Yang et al. *ApJ*, 984(1):15, May 2025. doi: 10.3847/1538-4357/adbbe8.

Y. Yuan, M. R. Krumholz, and C. L. Martin. *MNRAS*, 518(3):4084–4105, Jan. 2023. doi: 10.1093/mnras/stac3241.